Eur. Phys. J. B **45**, 207–212 (2005)
DOI: 10.1140/epjb/e2005-00051-5

THE EUROPEAN PHYSICAL JOURNAL B

Exchange coupling of bilayers and synthetic antiferromagnets pinned to MnPt

M. Rickart[1,a], A. Guedes[1], B. Negulescu[1], J. Ventura[2], J.B. Sousa[2], P. Diaz[3], M. MacKenzie[3], J.N. Chapman[3], and P.P. Freitas[1]

[1] INESC-MN, R. Alves Redol 9, 1000 Lisboa, Portugal
[2] IFIMUP, Universidade do Porto, R. Campo Alegre, 4100 Porto, Portugal
[3] Department of Physics and Astronomy, University of Glasgow, University Avenue, Glasgow, UK

Received 29 September 2004 / Received in final form 8 January 2005
Published online 8 March 2005 –

Abstract. Exchange bias and blocking temperature were studied in MnPt based bottom-pinned bilayers and synthetic antiferromagnets (SAF) prepared by magnetron sputtering. The structure and magnetic properties were determined as a function of the MnPt layer thickness. Exchange coupling was found to be (J_{ex} = 0.4 erg/cm^2) for a MnPt ($t \leq 20$ nm)/CoFe (5 nm) bilayer. The distribution of the blocking temperature T_B was analyzed and its width ΔT_B and center point $T_{B,\,center}$ determined. T_B is about 280 °C for thinner MnPt films, and increases to 330 °C for thick films. ΔT_B is constant for thick MnPt but steadily increases as the thickness decreases. SAF structures show higher exchange bias and higher $T_{B,\,center}$ at thin layer thickness ($t_{\mathrm{MnPt}} = 8.5$ nm) compared to bilayers.

PACS. 75.50.Ee Antiferromagnetics – 75.70.Cn Magnetic properties of interfaces (multilayers, superlattices, heterostructures) – 85.70.Kh Magnetic thin film devices: magnetic heads; domain-motion devices, etc.

1 Introduction

Several studies have dealt with the use of MnPt antiferromagnets (AF) as exchange bias layers in sensors, magnetic random access memories (MRAMs) and read heads [1–9]. In these devices the antiferromagnet is used to pin the magnetization of one of the two ferromagnetic (FM) layers, these layers being separated by a nonmagnetic spacer layer. The following summarizes the most important features required for a "perfect" antiferromagnet: the AF should provide a high exchange coupling to the pinned layer. High exchange bias should be maintained at the working temperature of the device, demanding a high thermal stability. A high resistivity is required to avoid current shunting in current-in-plane (CIP) spin valves. The properties of the antiferromagnet MnPt are superior compared to other antiferromagnets, but MnPt has a disadvantage: it is non-magnetic in the as-deposited state which has face-centered cubic (*fcc*) structural phase. It becomes antiferromagnetic after a structural transition to the ordered face-centered tetragonal (*fct*) phase upon annealing at elevated temperatures. A high degree of ordering during the phase transition depends on the right annealing conditions and is a prerequisite for enhanced exchange bias [10,11].

For read head application the AF layer should be as thin as possible (<10 nm), but high exchange bias as well as high thermal stability are difficult to maintain with thin layers. Exchange bias is reduced significantly for thin antiferromagnetic layers below t_{AF} = 10 nm and coercive fields become higher than exchange fields making such thin films unsuitable for devices. Also the blocking temperature decreases with decreasing thickness of the antiferromagnet [12,13]. Furthermore in a polycrystalline film each grain acts like a single particle having its own T_B. Therefore a distribution of blocking temperatures which can be attributed to the grains can be expected in a polycrystalline film. If a broad distribution is present in an AF, only some fraction of the AF grains will be in the range of the working temperature of the device. In the present study the blocking temperature distribution was analyzed to extract the center temperature $T_{B,\,center}$ of the distribution and its width ΔT_B. The main goal for high thermal stability of devices is therefore a high center temperature with a small width of the distribution, a configuration which is not yet achieved in the different antiferromagnetic materials available. The focus of this study lies in exchange bias and blocking temperature investigated as a function of the layer thickness of the antiferromagnet and related to the structural properties of the samples. The possibility of controlling the blocking temperature by the

[a] e-mail: rickart@physik.uni-kl.de

AF thickness is of special interest in new device designs where two exchange layers with different blocking temperatures are used for thermally assisted writing in MRAM cells [14].

An alternative to the FM/AF pinning mechanism in devices is the use of a synthetic antiferromagnet (SAF): two ferromagnetic layers separated by a non-magnetic metallic spacer (usually Ru) where one FM is pinned to an AF. The Ru thickness is chosen to obtain antiferromagnetic interlayer coupling of the two FM [15–18]. As a result high exchange bias in the order of several kOe is obtained and magneto-static coupling between the free and pinned layer, e.g. in nano-patterned device structures, is reduced.

2 Experimental

Exchange-coupled bottom-pinned bilayers Ta (7 nm)/Ru (3 nm)/$Mn_{51.5}Pt_{48.5}$ (t nm)/$Co_{90}Fe_{10}$ (5 nm)/Ta (3 nm) and SAF structures Ta (7 nm)/Ru (3 nm)/$Mn_{51.5}Pt_{48.5}$ (t nm)/$Co_{90}Fe_{10}$ (2.2 nm)/Ru (0.7 nm)/$Co_{90}Fe_{10}$ (3.2 nm)/Ta (3 nm) were prepared in an automated NORDIKO 2000 magnetron sputter system. The substrate was glass (CORNING 7059) coated with an Al (60 nm) buffer which was preheated at a set temperature of 150 °C for 30 min in vacuum and then ion-beam milled to reduce the surface roughness [19]. The films were sputtered from a composite target with a composition of $Mn_{63.6}Pt_{36.4}$ where additional Pt pieces were glued on top of the target to obtain a film composition of $Mn_{51.5}Pt_{48.5}$ as determined by Rutherford backscattering (RBS). Base pressure of the system was less than 5×10^{-8} mbar. Deposition pressure was 4.0–6.7 mbar using an Ar sputter gas with a flow rate of 10 sccm. The easy axis was set by applying a 20 Oe aligning field during deposition. To establish exchange bias the samples were annealed in vacuum ($<1\times10^{-5}$ mbar) with a rise time of 40 min to reach the set annealing temperature $T_A = 310$ °C for 2 h. A magnetic field of 3 kOe (5 kOe for the SAF samples) was applied along the easy direction of magnetization during anneal and furnace cool down. Additionally to the "standard" annealing method just described, some samples were rapid thermally annealed in UHV by a quartz lamp array without magnetic field: the temperature was increased within 3 min up to $T_{RTA} = 310$ °C and cool down was without applied magnetic field.

The structural phase of the MnPt layer was determined by X-ray diffraction (XRD) using Cu K_α radiation and the average out-of-plane grain size (D) calculated using Debye-Scherrer's equation. Transmission electron microscopy (TEM) studies of stacks in plan view and cross-section allowed investigation of both in-plane and out-of-plane grain size in the MnPt layer. The TEM studies were performed on an FEI Tecnai F20 operated at 200 kV. Magnetic properties were determined by M(H)-loops with a vibrating sample magnetometer (VSM) equipped with a heater for temperature dependent measurements in a temperature range from 25 °C to 400 °C.

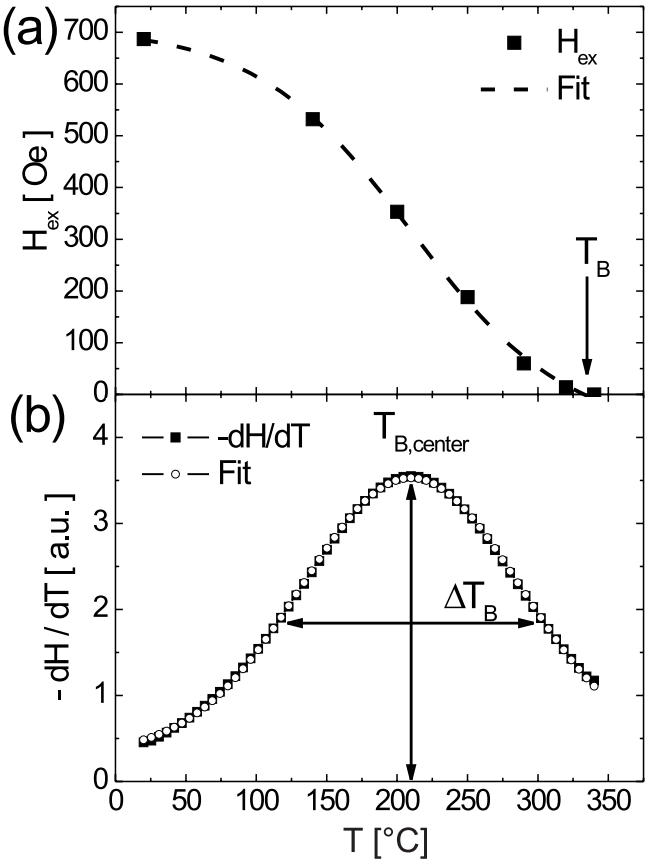

Fig. 1. Determination of $T_{B,\,center}$ and ΔT_B: Data points of the $H_{ex}(T)$-curve were fitted to derive the $-dH_{ex}/dT$-distribution. ΔT_B was determined at FWHM.

Data points in the $H_{ex}(T)$-curve were fitted with a Fermi-like function to derive the $-dH_{ex}/dT$-distribution and to determine the blocking temperature T_B as explained in Figure 1. The blocking temperature T_B is defined as the temperature where the exchange bias H_{ex} vanishes. This function was chosen because it provided a convenient way of fitting the data and supplied information about T_B and its distribution ΔT_B in a consistent manner for all MnPt/CoFe bilayers measured [20]. No physical meaning is intended by this fitting procedure.

3 Results and discussion

Figure 2 shows the exchange bias and coercive field of $Mn_{51.5}Pt_{48.5}$(t nm)/$Co_{90}Fe_{10}$ (5 nm) bilayers as a function of the AF layer thickness. The VSM measurements were performed at room temperature. A saturation value of $J_{ex} > 0.4$ erg/cm^2 is achieved for AF thicknesses higher than 20 nm ($J_{ex} = M_s \cdot t_{\mathrm{FM}} \cdot H_{ex}$ with $M_s(Co_{90}Fe_{10}) = 1200$ emu/cm^3 as measured for thin films). The crossover thickness where the coercive field H_c becomes larger than the exchange bias H_{ex} is determined to be $t_{cross} = 12.5$ nm which is similar to reference [7], although the bilayers investigated in the present study exhibit a higher exchange energy J_{ex}. The critical thickness where H_{ex}

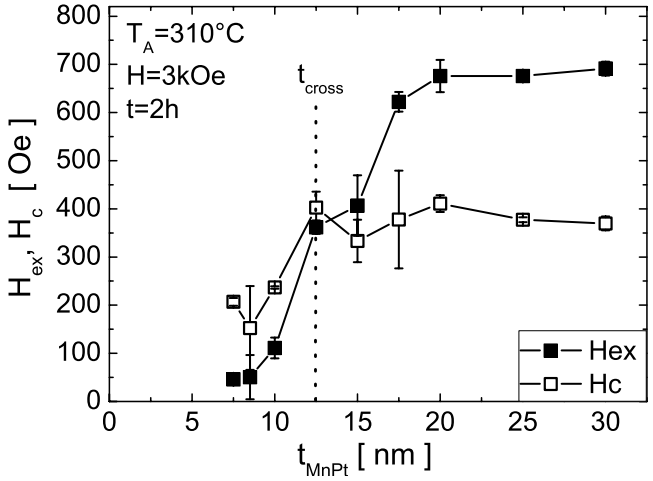

Fig. 2. Exchange bias H_{ex} and coercive field H_c dependences on the MnPt layer thickness. The crossover thickness t_{cross} was determined to be 12.5 nm. Annealing conditions for all samples were $T_A = 310$ °C, $H = 3$ kOe for 2 h.

becomes zero is 6 nm. Ultrathin MnPt films with a thickness lower than t_{cross} are therefore unsuitable for applications where a stable pinning direction of magnetization is required. Reference [11] also observed decreasing exchange bias with decreasing thickness of the AF. However, in the thinner samples investigated in reference [11] a mixture of *fcc* and *fct* MnPt phases was observed and the decrease in exchange bias with decreasing AF thickness was attributed to the presence of more residual *fcc* phase.

Figure 3a shows a typical ϑ-2ϑ XRD trace. The MnPt peak at $2\vartheta = 40.24°$ results from the Pt (111) layers and corresponds to *fct* structural phase. No *fcc* phase was observed for any layer thicknesses after annealing at $T_A = 310$ °C in $H = 3$ kOe for 2h [9]. In *fcc* phase the MnPt peak is observed at $2\vartheta = 39.88°$. Therefore the increase in exchange bias with AF layer thickness observed here cannot be attributed to increasing amounts of *fct* MnPt as in reference [11]. The average out-of-plane MnPt grain size (D) calculated from the XRD results is shown in Figure 3b as a function of layer thickness. D can be seen to rise with increasing layer thickness, with a trend towards saturation at $D \sim 18$ nm. Therefore an alternative explanation for the decrease of exchange bias as shown in Figure 2 possibly lies in the decrease in average grain size with decreasing AF thickness [21].

In order to obtain further information about the grain size in the films, a range of bilayers with MnPt thickness $t_{\mathrm{MnPt}} = 8.5$ nm, 20 nm and 30 nm were investigated by TEM. Figure 4 contains a bright field TEM image and a selected area electron diffraction pattern taken from a plan view as-deposited sample containing a 30 nm MnPt bilayer. While most of the rings in the diffraction pattern index as *fcc* MnPt, rings from the *fcc* CoFe and *hcp* Ru layers can also be identified. The (111) CoFe ring is present but relatively weak as a result of the (111) texture of this layer. The MnPt in the as-deposited sample was also textured with regularly shaped grains of the order of 10 nm size in-plane. The corresponding images and diffraction

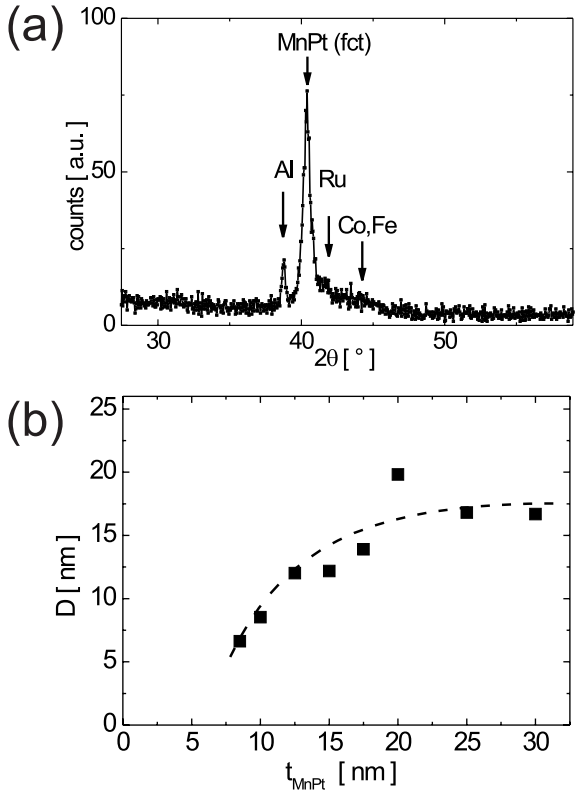

Fig. 3. (a) XRD trace of a sample with structure substrate/Al (60 nm)/Ta (7 nm)/Ru (3 nm)/$Mn_{51.5}Pt_{48.5}$ (30 nm)/$Co_{90}Fe_{10}$ (5 nm)/Ta (3 nm). (b) Grain size D determined from XRD as function of the MnPt layer thickness in bilayers with same structure as in (a). The dashed line is a guide to the eyes.

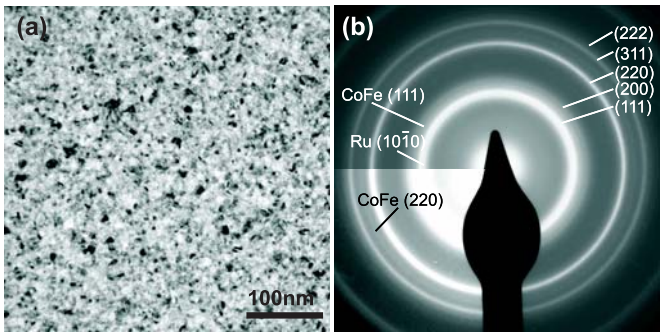

Fig. 4. (a) Bright field TEM image and (b) selected area diffraction pattern of an as-deposited bilayer containing a 30 nm MnPt layer. The rings indexed on the right hand side of the diffraction pattern correspond to the *fcc* MnPt phase.

patterns from MnPt bilayers after annealing are shown in Figure 5. In agreement with the XRD results, the rings in the diffraction patterns index as *fct* MnPt, *fcc* CoFe and *hcp* Ru. If both MnPt phases were present in a sample, the *fcc* phase could be identified by its (220) reflection which would appear between the (220) and (202) reflections of the *fct* phase. As there is no evidence of the presence of the *fcc* (220) reflection in the diffraction patterns after annealing, we conclude that there is no significant amount

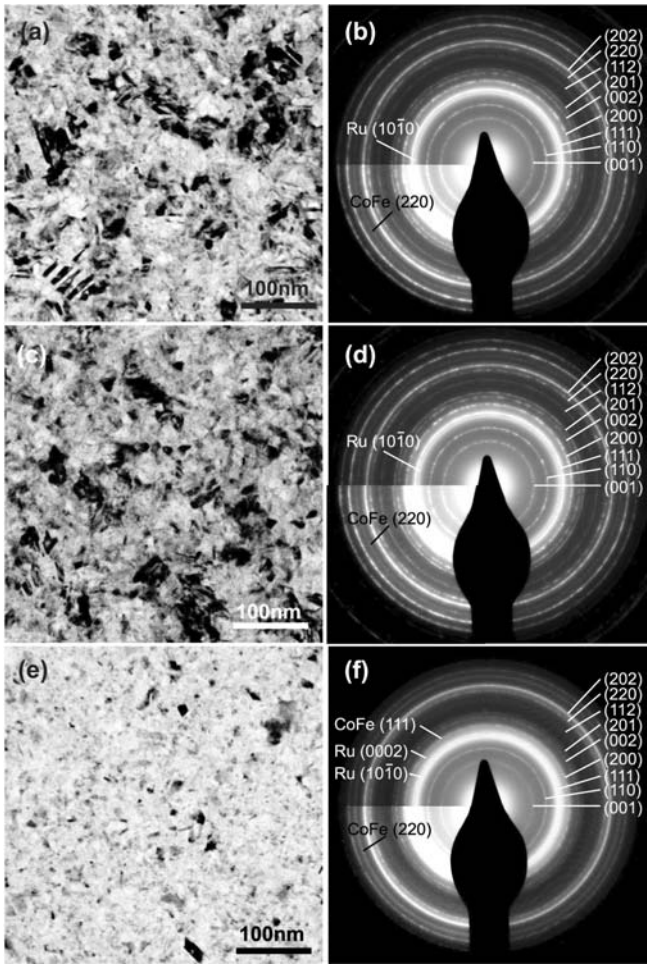

Fig. 5. Bright field TEM images and selected area diffraction patterns of (a) and (b) a rapid thermally annealed (T_{peak} = 300 °C, t = 3 min) bilayer containing a 30 nm MnPt layer, (c) and (d) a standard annealed (T = 310 °C, H = 5 kOe, t = 2 h) bilayer containing 30 nm MnPt layer, (e) and (f) a standard annealed (T = 310 °C, H = 5 kOe, t = 2 h) bilayer containing an 8.5 nm MnPt layer. The rings indexed on the right hand side of the diffraction patterns correspond to the *fct* MnPt phase.

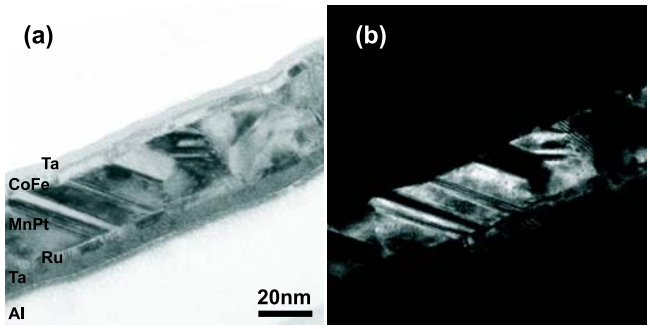

Fig. 6. (a) Bright field and (b) dark field cross-sectional TEM images of a bilayer containing a 30 nm MnPt layer after a standard anneal.

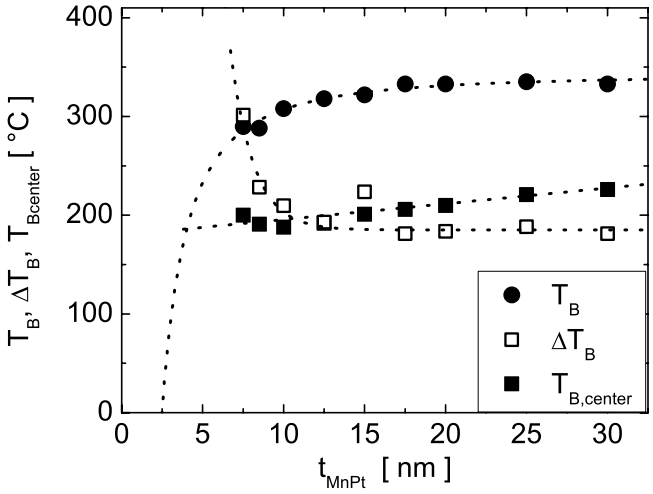

Fig. 7. Blocking temperature T_B (black dots), center of blocking temperature distribution $T_{B,center}$ (black squares), distribution ΔT_B (black hollow squares) as function of the MnPt thickness (the dotted lines are guides to the eye).

of residual *fcc* MnPt present. The results from the 30 nm bilayers after a standard anneal and after a rapid thermal anneal are similar: in both cases the MnPt grains lose their texture, become more complex in shape, exhibit twinning and have a larger distribution of sizes ranging roughly between about 10 nm and 100 nm in-plane. However, results from the 8.5 nm MnPt bilayer after a standard anneal were different: the MnPt layer retained some texturing and while the in-plane grains looked less complex than those observed in the 30 nm annealed bilayers they were less uniform in size and shape than those in the as-deposited layer.

Cross-sectional TEM studies were made of a 20 nm as deposited bilayer and 30 nm, 20 nm and 8.5 nm MnPt bilayers after annealing. These studies showed that while many of the grains in the annealed MnPt layers were columnar there were also regions in the 20 nm and 30 nm films where the grains were not continuous through the layer thickness. Thus the average out-of-plane grain size must be less than the MnPt thickness in these samples. This is in agreement with the XRD measurements where saturation in average out-of-plane grain size was observed at ∼18 nm. Figure 6 of a 30 nm bilayer in cross-section illustrates the complex grain structure. The cross-sectional TEM studies also showed that there was some correlation between the topography of the MnPt layer surface and the roughness of the underlying Al buffer layer.

The blocking temperature for each thickness was determined by the $H_{ex}(T)$-curve (Fig. 1a). From the dH_{ex}/dT-curve the center temperature $T_{B,\,center}$ and the width ΔT_B of the distribution was evaluated as shown in Figure 1b. The results for all thicknesses are displayed in Figure 7. Relatively high blocking temperatures with values above T_B = 300 °C were obtained for MnPt thicknesses greater than 10 nm. $T_{B,\,center}$ decreases marginally, while the width ΔT_B of the distribution increases with decreasing thickness of the antiferromagnet. According to this analysis of the blocking temperature distribution, for thin MnPt layers some grains exhibit T_B lower than room

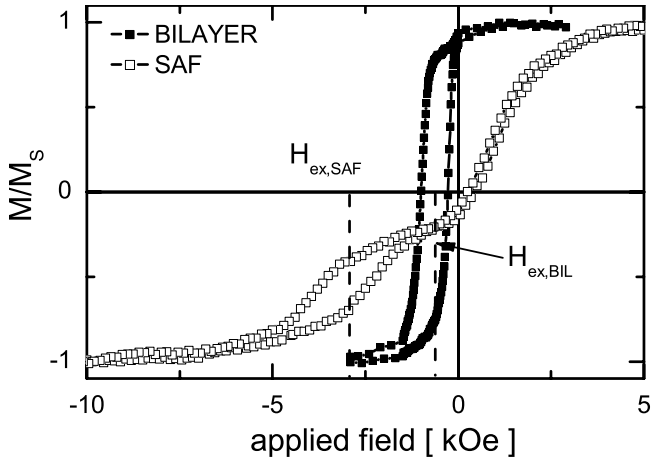

Fig. 8. M(H)-loops of a bilayers with structure glass/Al (60 nm)/Ta (7 nm)/Ru (3 nm)/$Mn_{51.5}Pt_{48.5}$ (25 nm)/$Co_{90}Fe_{10}$ (5 nm)/Ta (3 nm) and a SAF sample with structure glass/Al (60 nm)/Ta (7 nm)/Ru (3 nm)/$Mn_{51.5}Pt_{48.5}$ (25 nm)/$Co_{90}Fe_{10}$ (2.2 nm)/Ru (0.7 nm)/$Co_{90}Fe_{10}$ (3.2 nm)/Ta (3 nm). Samples were annealed at $T_A = 310$ °C in a field of 3 kOe (5 kOe for SAF) for 2 h.

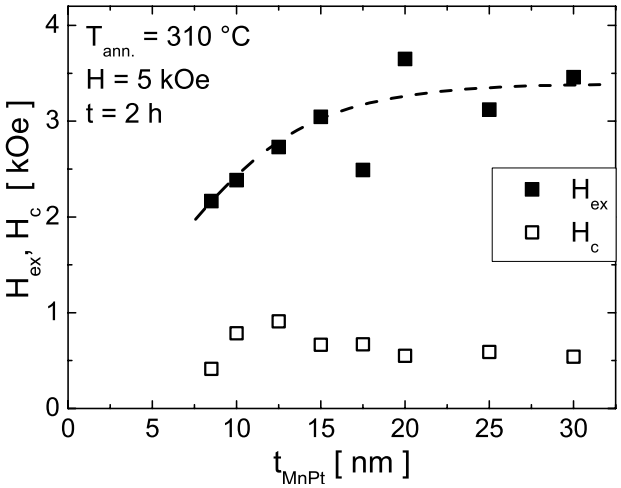

Fig. 9. Exchange bias H_{ex} and coercive field H_c dependence on the MnPt layer thickness of SAF samples with structure glass/Al (60 nm)/Ta (7 nm)/Ru (3 nm)/$Mn_{51.5}Pt_{48.5}$ (t nm)/$Co_{90}Fe_{10}$ (2.2 nm)/Ru (0.7 nm)/$Co_{90}Fe_{10}$ (3.2 nm)/Ta (3 nm). High pinning strength was preserved to a thickness of the antiferromagnet down to 8.5 nm. The dashed line is a guide to the eyes.

temperature. These crystallites do not contribute to the exchange bias at room temperature. Therefore the H_{ex} for thin layers might be underestimated in Figure 2. This does not apply for thick layers where ΔT_B suggests all grains contribute to exchange bias at room temperature. The disorder in blocking temperatures represented by the width ΔT_B can be attributed to less pinning strength for thin MnPt layer thicknesses and a large distribution of coercive fields at room temperature as shown in Figure 2 [22]. Thus the increase of the width of blocking temperature distribution for the thinner MnPt layers can be related to changes in the out-of-plane and in-plane grain sizes connected with distributed magnetocrystalline anisotropies [21–23]. On the other hand the center temperatures $T_{B,\,center}$ are much higher than those of other antiferromagnets, such as IrMn or FeMn, which favor MnPt for devices working in an ambient with high temperatures [22].

As already mentioned in Section I SAF structures (two FM layers separated by a metallic spacer layer e.g. Ru, where one FM layer is pinned by an AF) can be introduced to improve the pinning strength. In terms of high density read head application, for example, a minimum AF layer thickness of $t = 10$ nm is already large [24]. In this study the exchange bias, blocking temperature and distribution of the SAF structures was investigated in the same way as the study on the bilayer structures. The investigated sample had the structure: glass/Ta (7 nm)/Ru (3 nm)/$Mn_{51.5}Pt_{48.5}$ (t nm)/$Co_{90}Fe_{10}$ (2.2 nm)/Ru (0.7 nm)/$Co_{90}Fe_{10}$ (3.2 nm)/Ta (3 nm). A comparison of the M(H)-loops of a bilayer and a SAF structure, both with a MnPt layer thickness of 25 nm, is shown in Figure 8. The exchange bias of the SAF structure is due to the strong antiferromagnetic interlayer coupling between the two CoFe layers across the Ru layer, about 5 times higher than the H_{ex} of the bilayer. Figure 9 shows the exchange bias H_{ex} as a function of the MnPt thickness. Values of $H_{ex} \sim 3$ kOe were obtained for MnPt thicknesses higher than 15 nm. Compared to simple bilayer structures, the MnPt thickness can be lowered down to 8.5 nm using a SAF structure while maintaining a significant pinning ($H_{ex} \sim 2$ kOe). At elevated temperatures ($T = 300$ °C) the H_{ex} has decreased significantly but is still around 1 kOe. This thermal stability allows a reduction of the total thickness of the bottom electrode from 25 nm in the bilayer ($Mn_{51.5}Pt_{48.5}$ (20 nm)/$Co_{90}Fe_{10}$ (5 nm)) to 14.6 nm in a bottom electrode with SAF structure ($Mn_{51.5}Pt_{48.5}$ (8.5 nm)/$Co_{90}Fe_{10}$ (2.2 nm)/Ru(0.7 nm)/$Co_{90}Fe_{10}$ (3.2 nm)). Table 1 shows the values of the exchange strength and the blocking temperatures of SAF structures for various MnPt thicknesses. T_B was found to be similar to the bilayers. On the other hand the center temperature shifts due to the strong interlayer coupling to higher values around $T_{B,\,center} \sim 300$ °C [3]. The distribution width ΔT_B has similar values compared to bilayers (not shown). For a comparison of the thermal stability of a bilayer and a SAF as shown in Figure 10, a better parameter such as the change of the exchange field with temperature near the blocking temperature, e.g. $dH_{ex}/dT(T \sim 300$ °C) has to be taken into account. This is more significant for SAF than for bilayers. Thus devices using SAF with reduced AF thickness show a higher degree of thermal stability and can be operated at high temperatures without losing their pinning strength.

4 Conclusions

High exchange coupling of $J_{ex} = 0.4$ erg/cm^2 was obtained for bilayer structures containing MnPt as the antiferromagnet. For MnPt thicknesses higher than 20 nm the

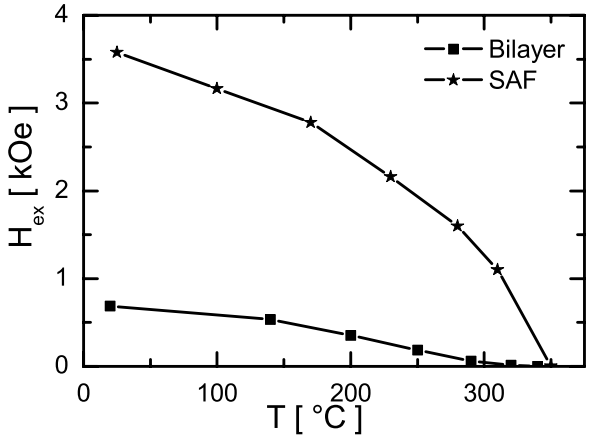

Fig. 10. Exchange bias H_{ex} dependence on the temperature of a SAF sample (black stars) with structure glass/Al (60 nm)/Ta (7 nm)/Ru (3 nm)/$Mn_{51.5}Pt_{48.5}$ (20 nm)/$Co_{90}Fe_{10}$ (2.2 nm)/Ru (0.7 nm)/$Co_{90}Fe_{10}$ (3.2 nm)/Ta (3 nm) and a bilayer (black squares) with structure glass/Al (60 nm)/Ta (7 nm)/Ru (3 nm)/$Mn_{51.5}Pt_{48.5}$ (20 nm)/$Co_{90}Fe_{10}$ (5 nm)/Ta (3 nm). The slope of the SAF curve around $T = 300$ °C (near T_B) is significantly higher compared to the bilayer.

Table 1. H_{ex}, T_B, $T_{B,center}$ as function of t_{MnPt} for the SAF structures.

t_{MnPt} (nm)	H_{ex} (kOe)	T_B (°C)	$T_{B,\,center}$ (°C)
8.5	2.2	280	∼275
12.5	2.4	310	∼295
15	3.0	345	335
20	3.5	333	328
30	3.5	335	333

exchange coupling was constant. The crossover thickness of the antiferromagnet, where unstable pinning occurred, was 12.5 nm. Blocking temperatures were measured as a function of the thickness of the antiferromagnet. A bulk blocking temperature of $T_B \sim 340$ °C was determined. The width of the blocking temperature distribution was found to increase with decreasing MnPt thickness, whereas the center temperature of the distribution decreased slightly with decreasing thickness with a value around $T_{B,\,center} = 210$ °C. Samples with SAF structure showed high exchange bias fields, around 3 kOe, for all thicknesses of the MnPt layer. T_B for the SAF was found to be higher and ΔT_B lower than for bilayer structures. SAF samples with MnPt thickness of 8.5 nm showed stable pinning and high blocking temperature making them favorable for read head applications.

M.R. acknowledges the financial support from the European Communities Human Potential Programme NEXBIAS under the contract number (HPRN-CT2002-00296). The authors would like to thank F. Silva and J. Bernardo (Inesc-MN) for technical support. The work also is supported in part by the European Communities Human Potential programme under contract number HRPN-CT-2002-00318 ULTRASWITCH and by Scottish Enterprise. The authors would like to thank Mr B Miller (University of Glasgow) for preparing the cross-sectional TEM specimens.

References

1. R.F.C. Farrow, R.F. Marks, S. Gider, A.C. Marley, S.S.P. Parkin, D. Mauri, J. Appl. Phys. **81**, 4986 (1997)
2. K.M. Krishnan, C. Nelson, C.J. Echer, R.F.C. Farrow, R.F. Marks, A.J. Kellock, J. Appl. Phys. **83**, 6810 (1998)
3. G.W. Anderson, Y. Huai, M. Pakala, J. Appl. Phys. **87**, 5726 (2000)
4. G.W. Anderson, M. Pakala, Y. Huai, IEEE Trans. Mag. **36**, 2605 (2000)
5. S. Mao, Z. Gao, IEEE Trans. Mag. **36**, 2860 (2000)
6. Z.T. Diao et al., IEEE Trans. Mag. **36**, 2632 (2000)
7. J.K. Kim, S.-R. Lee, S.A. Song, G.-S. Park, H.S. Yang, K.-I. Min, J. Appl. Phys. **89**, 6907 (2001)
8. C.-L. Lee, A. Davasahayam, M. Mao, J. Kools, P. Cox, K. Masaryk, D. Mahenthiran, J. Munson, J. Appl. Phys. **93**, 8406 (2003)
9. M. Rickart, P.P. Freitas, I.G. Trindade, N.P. Barradas, E. Alves, M. Salgueiro, N. Muga, J. Ventura, J.B. Sousa, G. Proudfoot, D. Pearson, M. Davis, J. Appl. Phys. **95**, 6317 (2004)
10. T. Pokhil, E. Linville, S. Mao, J. Appl. Phys. **89**, 6588 (2001)
11. M.F. Toney, M.G. Samant, T. Lin, D. Mauri, Appl. Phys. Lett. **81**, 4565 (2002)
12. P.J. van der Zaag, Y. Ijiri, J.A. Borchers, L.F. Feiner, R.M. Wolf, J.M. Gaines, R.W. Erwin, M.A. Verheijen, Phys. Rev. Lett. **84**, 6102 (2000)
13. H. Xi, B. Bian, D.E. Laughlin, R.M. White, J. Appl. Phys. **87**, 4918 (2000)
14. J. Wang, P.P. Freitas, Appl. Phys. Lett. **84**, 945 (2004)
15. S.S.P. Parkin, N. More, K.P. Roche, Phys. Rev. Lett. **64**, 2304 (1990)
16. D. Heim, S.S.P. Parkin, U.S. Patent No. 5 465 185
17. B. Dieny, M. Li, S.H. Liao, C. Horng, K. Ju, J. Appl. Phys. **87**, 3415 (2000)
18. I.L. Prejbeanu, W. Kula, K. Ounadjela, R.C. Sousa, O. Redon, B. Dieny, J.-P. Nozières, IEEE Trans. Mag. **40**, 2625 (2004)
19. S. Cardoso, Z.G. Zhang, P.P. Freitas, P. Wei, N. Barradas, J.C. Soares, J. Appl. Phys. **89**, 6650 (2001)
20. For antiferromagnetic materials different to MnPt the use of a Fermi-like function to fit the H_{ex} vs. temperature might not be appropriate
21. K. Nishioka, S. Shigematsu, T. Imagawa, Sh. Narishige, J. Appl. Phys. **83**, 3233 (1998)
22. J.P. Nozières, S. Jaren, Y.B. Zhang, A. Zeltser, K. Pentek, V.S. Speriosu, J. Appl. Phys. **87**, 3920 (2000)
23. K. Nishioka, C. Hou, H. Fujiwara, R.D. Metzger, J. Appl. Phys. **80**, 4528 (1996)
24. A.J. Devasahayam, M.H. Kryder, IEEE Trans. Mag. **35**, 649 (1999)